A Compact Reconfigurable NRI-TL Metamaterial Phase-Shifter for Antenna Applications

A Compact Reconfigurable NRI-TL Metamaterial Phase-Shifter for Antenna Applications

Muhammad Ali Babar Abbasi, Marco A. Antoniades, and Symeon Nikolaou

***Abstract*—This paper presents a compact reconfigurable phase-shifter based on negative-refractive-index transmission-line (NRI-TL) metamaterial unit cells. Two inter-switchable NRI-TL metamaterial unit cells are collocated within the same board area, and can be reconfigured based on the biasing polarity of embedded PIN diodes to provide two discrete phase states. The PIN diodes are located on the shunt branches of the metamaterial line in order to reduce losses in the direct signal path. Design limitations in terms of return loss and insertion loss are discussed in relation to the two phase states. A proof-of-concept module with a size of 17.8 × 21.6 mm2 is designed at 1 GHz, with measured insertion phases of −14.5° and +58.5° in the two phase states leading to a differential phase shift of 73°, while exhibiting insertion losses of 1.43 dB and 0.89 dB, respectively. The combined bandwidth for which the reflection coefficient in both states remains simultaneously below −10 dB is 0.46 GHz (46%), from 0.83 GHz to 1.29 GHz.**

***Index Terms*— Negative-refractive-index transmission-line (NRI-TL), reconfigurable, metamaterial, phase shifter.**

I. Introduction

Artificial material engineering has enabled the design and development of compact, cost-effective and high-performance solutions at microwave, terahertz and optical frequencies. The electromagnetic behavior of metamaterial structures is modified intentionally by adjusting either their electrical or geometrical properties to formulate non-linear materials, semiconductor structures, liquid crystals, microfluids and so on [1]. Within the same framework, the increasing demand for tunable microwave systems for advanced steerable antenna array systems has further advanced research towards reconfigurability within metamaterials. At microwave frequencies, recent developments in negative-refractive-index transmission line (NRI-TL) metamaterials [2-3] have enabled the design and realization of electrically small reconfigurable metamaterial lines. The reconfigurability is achieved by loading a host transmission line with adjustable lumped capacitors and inductors. The practical use of such NRI-TL metamaterials still poses a number of technological and theoretical challenges in terms of operational bandwidth, losses, realization complexity, tuning speed and tolerance sensitivity. Over and above the aforementioned challenges, the inclusion of the tuning mechanism (biasing lines and control mechanism) must not affect the desired electromagnetic behavior of the reconfigurable system. Traditionally, ferrites have been used to achieve continuous phase shifting in antenna array systems [4-5], but more recently other novel materials such as graphene have also been used [6].

Some prominent techniques to achieve reconfigurability in metamaterial phase shifters include microfluidic channels [7], mechanically variable MIM capacitors [8], CMOS-based active inductors [9-10], BST thick-film substrates [11], GaAs [12-13] and Schottky varactor diodes [14], ferroelectric varactors [15], and MEMS capacitors [16].

In this work, a reconfigurable NRI-TL metamaterial phase shifter is presented that uses PIN diodes to change the insertion phase through the device. Two phase states have been achieved by reciprocating the polarity of the biasing voltage. Using the same physical microstrip transmission line to host more than one NRI-TL metamaterial unit cells, leads to a degradation in the performance of the phase shifter when switching from one state to another. These issues are thoroughly discussed, leading to the major contribution of this work, which is the application of a multivariable optimization algorithm that allows the device to exhibit low insertion loss and good impedance matching for both phase states. A detailed analysis related to design limitations and the matching topology used to match both phase states in a common design is presented in the following sections.

II. Proposed Reconfigurable NRI-TL Metamaterial

NRI-TL metamaterials are synthesized by periodically loading a conventional microwave transmission line with lumped-element series capacitors and shunt inductors. Fig. 1(a) shows the equivalent circuit of a symmetric Π-shaped NRI-TL metamaterial unit cell [17]. Here, a host transmission line with characteristic impedance Z_0, series inductance per unit length L, shunt capacitance per unit length C, and length d has been loaded with a lumped-element series capacitor C_0 and two shunt inductors $2L_0$. The conventional host transmission line realizes a negative phase response, $\phi_{H\text{-}TL}$, while the series capacitive and shunt inductive loading forms a backward-wave (BW) line with a positive phase response, ϕ_{BW}, as shown in Fig. 1(b). Under effective medium conditions, the phase shift per NRI-TL metamaterial unit cell is given by [3]:

$$\phi_{MTM} = \phi_{H-TL} + \phi_{BW} \tag{1a}$$

$$\phi_{MTM} = -\omega\sqrt{LC}d + \frac{1}{\omega\sqrt{L_0 C_0}} \tag{1b}$$

This is valid under the impedance matching condition below, which stipulates that both the lines must have the same characteristic impedance.

$$Z_0 = \sqrt{\frac{L}{C}} = \sqrt{\frac{L_0}{C_0}} \tag{2}$$

Manuscript received April 27, 2017 and revised September 30, 2017. This work was supported in part by the European Union through the Erasmus Mundus INTACT Doctorate Level Mobility program.

M. A. B. Abbasi and S. Nikolaou are with the Department of Electrical Engineering,Frederick University, 1036 Nicosia, Cyprus (e-mail: m.babarabbasi@gmail.com; s.nikolaou@frederick.ac.cy).

M. A. Antoniades is with the Department of Electrical and Computer Engineering, University of Cyprus, 1678 Nicosia, Cyprus (e-mail: mantonia@ucy.ac.cy).

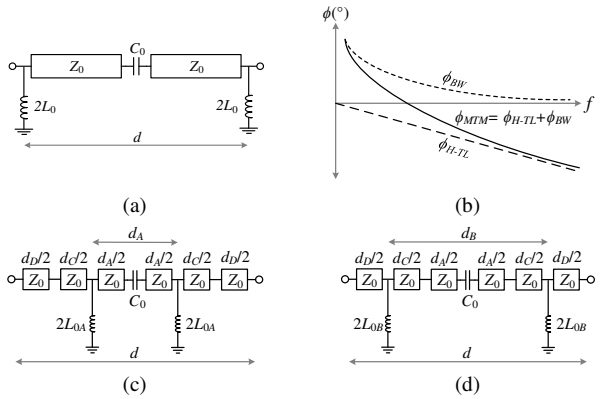

Fig.1 (a) NRI-TL metamaterial Π unit cell, (b) phase response of a metamaterial line as a composite response of the transmission line (TL) and backward-wave (BW) line responses, and metamaterial line architecture for (c) phase *State A*, and (d) phase *State B* (d_D represents an extra length of feeding transmission line outside the unit cells).

In this work, a microstrip transmission line with an impedance of $Z_0 = 50\ \Omega$ and a fixed length of $d = 35$ mm is used to host two collocated and reconfigurable NRI-TL metamaterial phase-shifting lines that realize two discrete phase states, *State A* and *State B*, given by ϕ_{MTM_A} and ϕ_{MTM_B}, respectively. The architecture of the two individual NRI-TL metamaterial lines is shown in Fig. 1(c) and (d). Both lines have the same series components, and differ only in the locations and values of the shunt loading inductors, L_{0A} and L_{0B}. By switching between the two inductor values, a fixed phase change can be effected, according to (1b). A change in the value of L_0 without changing C_0, however, will lead to a mismatch along the line, since the impedance matching condition of (2) will no longer apply. This is mitigated by the fact that the two metamaterial unit cells used in Fig. 1 (c) and (d) also differ in size, given by d_A and d_B respectively, providing an additional degree of freedom that is used to provide good impedance matching in both states. Note that the total length of both the metamaterial lines (including the feed lines) always remains fixed at $d = d_A + d_C + d_D = 35$ mm.

III. Reconfigurable Phase Shifter Design

Initially, the structure of Fig. 1(a) was used to design a two-state NRI-TL metamaterial line with a fixed length. Using (1) and the design procedure outlined in [17], p. 17 with $\phi_{H\text{-}TL} = -70°$ at a design frequency of $f_0 = 1$ GHz, the loading element values required to achieve a phase of $\phi_{MTM\_A} = -15°$ in *State A* are $C_0 = 3.2$ pF, and $L_0 = 8.0$ nH, while to achieve a phase of $\phi_{MTM\_B} = +60°$ in *State B* the values are $C_0 = 1.4$ pF, and $L_0 = 3.5$ nH. The values for the phases ϕ_{MTM_A} and ϕ_{MTM_B} were chosen representatively in order to realize a proof-of-concept design with two phase states that are not harmonically related. The transmission and reflection characteristics of the two-state metamaterial line are presented in Fig. 2. It can be observed from Figs 2(a) and 2(b) that in both states the metamaterial line exhibits excellent transmission and reflection characteristics around 1 GHz, while the two desired phase states are achieved.

Combining two NRI-TL metamaterial lines representing two distinct phase states poses two major challenges. Firstly, when the same transmission line is used to host two NRI-TL unit cells

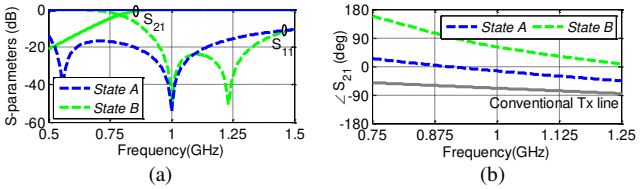

Fig. 2. Simulated responses for (a) magnitude of S-parameters, and (b) phase of S_{21} when the NRI-TL metamaterial line of Fig. 1 (a) is designed to incur $\phi_{MTM\_A} = -15°$ in *State A* and $\phi_{MTM\_B} = +60°$ in *State B*, compared to the same length conventional transmission line.

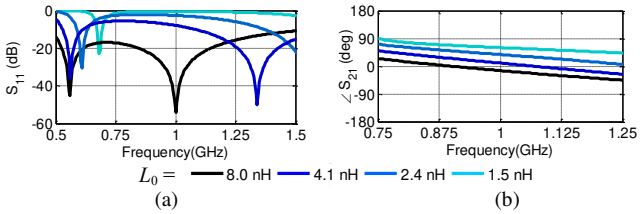

Fig. 3. Simulated responses for (a) $|S_{11}|$, and (b) phase of S_{21} of the NRI-TL metamaterial line as the value of the shunt loading inductor L_0 is varied from 8.0 nH in *State A* with a phase of $\phi_{MTM\_A} = -15°$ to 1.5 nH in *State B* with a phase of $\phi_{MTM\_B} = +60°$. The length of the unit cell size, d, and the loading capacitance, C_0, remain the same i.e. $\phi_{H\text{-}TL} = -70°$, $f_0 = 1$ GHz, and $C_0 = 3.2$ pF.

with reconfigurability only in the shunt branch, a single series loading capacitor C_0 must be used for both phase states, which results in impedance matching degradation. To further elaborate on this, consider the NRI-TL metamaterial unit cell from above that incurs a phase of $\phi_{MTM\_A} = -15°$ at 1 GHz in *State A*, that is now required to change its phase to $\phi_{MTM\_B} = +60°$ at 1 GHz in *State B* without changing the value of C_0. In order to increase the phase incurred to achieve a higher phase in *State B* using the same unit cell size and series capacitive loading, the shunt loading inductance L_0 must be decreased according to (1b), since $\phi_{H\text{-}TL}$ and C_0 will remain constant. The gradual decrease in the value of L_0 that leads to a higher incurred phase can be seen clearly in Fig. 3, together with the commensurate degradation of the impedance matching at 1 GHz. This is due to the mismatch between the characteristic impedance of the transmission line (50 Ω) and the backward-wave line (21.7 Ω), which makes the impedance matching condition of (2) invalid. The second major challenge in the implementation of the two-state phase shifter is that a reconfigurable mechanism is required that does not disturb the matching and phase response of the metamaterial line while switching between the two phase states.

The proposed reconfigurable NRI-TL metamaterial phase-shifter shown in Fig. 4 resolves both these problems. The phase-shifting line consists of a microstrip transmission line with a series loading capacitor C_0, and two pairs of reconfigurable shorted stubs, namely *Stub A* ($l_{A1}+l_{A2}+l_{A3}$) and *Stub B* ($l_{B1}+l_{B2}+l_{B3}$), which host the shunt loading inductors $2L_{0A}$ and $2L_{0B}$, and which are placed in shunt at fixed distances along the transmission line. The two main functions of these stubs are to facilitate the reconfigurability mechanism enabling them to switch between the two discrete shunt inductor loading values, and to aid in impedance matching.

The metamaterial phase-shifter of Fig. 4 was first designed in the Keysight – Advanced Design System (ADS) simulator as shown in Fig. 5 to incur an insertion phase in *State A* of $\phi_{MTM\_A} = -15°$ at 1 GHz using the two central stubs (*Stub A*), while the

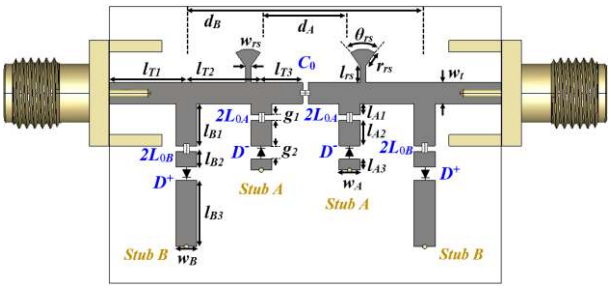

Fig. 4. Layout configuration of the two-state reconfigurable NRI-TL metamaterial phase shifter.

TABLE I
DIMENSIONS OF THE PHASE-SHIFTER LAYOUT SHOWN IN FIG. 4

parameter	Length (mm)	parameter	Length (mm)	parameter	Length (mm)
l_{T1}	6.95	l_{A1}	1.00	w_A	1.90
l_{T2}	6.80	l_{A2}	2.30	w_{rs}	0.50
l_{T3}	3.75	l_{A3}	1.00	g_1	0.50
l_{B1}	3.80	l_{rs}	1.49	g_2	1.20
l_{B2}	1.40	w_t	1.90	r_{rs}	1.50
l_{B3}	6.00	w_B	1.90	θ_{rs}	70°

two outer stubs (*Stub B*) were turned off. Subsequently, the two outer stubs (*Stub B*) were turned on, and the two inner ones (*Stub A*) were turned off while keeping C_0 constant, in order to achieve an insertion phase in *State B* of ϕ_{MTM_B} = +60° at 1 GHz, thus achieving a differential phase shift of 75°. In doing so, a similar impedance matching degradation to the one shown in Fig. 3(a) was observed. Thus, Quasi-Newton multivariable optimization was used to match the impedance of both *State A* and *State B* using the following algorithm.

IV. OPTIMIZATION ALGORITHM

Step 1: For phase *State A*, design a metamaterial unit cell on a transmission line with an impedance Z_0, length d, phase shift ϕ_{MTM_A} at frequency f_0, and formulate initial C_0 and L_{0A} values.
Step 2: Design stub A with lengths L_A1, L_A2 and L_A3 and gaps to host L_{0A} and PIN diode with forward polarity.
Step 3: For phase *State B*, calculate L_{0B} for phase shift ϕ_{MTM_B} while C_0 is kept the same as defined in Step 1.
Step 4: Design stub B with lengths L_B1, L_B2 and L_B3 and gap to host L_{0B} and PIN diode with reverse polarity.
Step 5: Evaluate optimized values of the *optimization variables* using Quasi-Newton multivariable optimization with the following simultaneous goals:

1. $|S_{11}|$ in *State A* < −10 dB at f_0
2. $|S_{11}|$ in *State B* < −10 dB at f_0
3. ∠ S_{21} in *State A* = $\phi_{MTM\_A} \pm E_A$°
4. ∠ S_{21} in *State B* = $\phi_{MTM\_B} \pm E_B$°
5. 2 × (TL_L1+TL_L2+TL_L3) = d

(Where E_A and E_B are the tolerance factors in degrees with initial value = 0.5°)

If the optimization criteria are satisfied go to the next sequential step. Else go to Step 14.
Step 6: Define *optimization variables* L_B1, LB_2, LB_3, L_A1, L_A2 and L_A3. Go to Step 5. If already optimized, go to next sequential step.
Step 7: Define *optimization variables* TL_L1, TL_L2, TL_L3. Repeat Step 5 and 6. If already optimized, go to next sequential step.
Step 8: Define *optimization variables* L_{0A} and L_{0B}. Repeat Step 5, 6 and 7.
Step 9: Replace the optimized values of L_{0A} and L_{0B} with closest discrete inductance value from the Coilcraft chip inductor library. Repeat Step 5, 6 and 7.
Step 10: Define *optimization variables* C_0. Repeat Step 5, 6 and 7.
Step 11: Replace the optimized value of C_0 with closest discrete capacitance value from the Murata chip capacitor library. Repeat Step 5, 6 and 7.
Step 12: Define *optimization variables* RS_L1, RS_L2, RS_W, RS_theta. Repeat Step 5, 6 and 7.
Step 13: Decrease E_A and E_B values by 0.5°. Repeat Steps 6-12. If already optimized in previous iteration, go to Step 15.
Step 14: Increase E_A and E_B values by 0.5°. Repeat Step 6-12.
Step 15: End.

The algorithm was used with the following inputs: Z_0 = 50 Ω, d = 35 mm ϕ_{MTM_A} = −15° (*State A*), ϕ_{MTM_B} = +60° (*State B*) and f_0 = 1 GHz. Upon successful completion of the optimization algorithm, the final values of the lumped components were C_0 = 3.10 pF, L_{0A} = 0.55 nH, L_{0B} = 1.40 nH, while the optimized geometrical dimensions of the phase shifter are listed in Table I. The resulting phase difference between states A and B was 73°. The proposed algorithm works for a given ϕ_{MTM_A} and ϕ_{MTM_B} and the error tolerance factors E_A and E_B can be set based on the application in which the proposed model is to be used. For the scenario discussed in section III, the final values of E_A and E_B were 1.5°.

V. FABRICATION

To achieve reconfigurability, a Skyworks SMP1345 PIN diode was used, which achieves ON and OFF states based on the biasing polarity. It is important to note that the polarity of the diode on *Stub A* (D^-) is opposite to the polarity of the diode on *Stub B* (D^+). Negative biasing through the radial stubs (l_{rs}, w_{rs}, r_{rs}, and θ_{rs}) along the top of the microstrip line in Fig. 4 turns on the two diodes D^-, and turns off the two diodes D^+, thus defining *State A*. Similarly, positive biasing through the radial stubs reverses this operation, consequently defining *State B*. The DC ground for the differential diode biasing voltage is applied on the microstrip ground and is applied to the diodes through the grounding vias at the end of the stubs.

Surface-mount Murata chip capacitors (GJM03 series) and Coilcraft chip inductors (0402CS series), both with high self-resonant frequencies well above the operating frequency, were used in the realization of the phase shifter. It is important to mention that the achievable phase states rely on the available lumped-element component values in the Murata GJM03 series and the Coilcraft 0402CS series component libraries. The gaps g_1 and g_2 wre designed keeping in mind the recommended soldering footprint for each lumped-element component and the diodes.

Finally, Keysight – ADS was used to design and analyze the performance of the proposed reconfigurable NRI-TL phase shifter using realistic S-parameter models for the Murata capacitors, the Coilcraft inductors and the Skyworks diodes, in conjunction with a realistic model of the physical geometry of

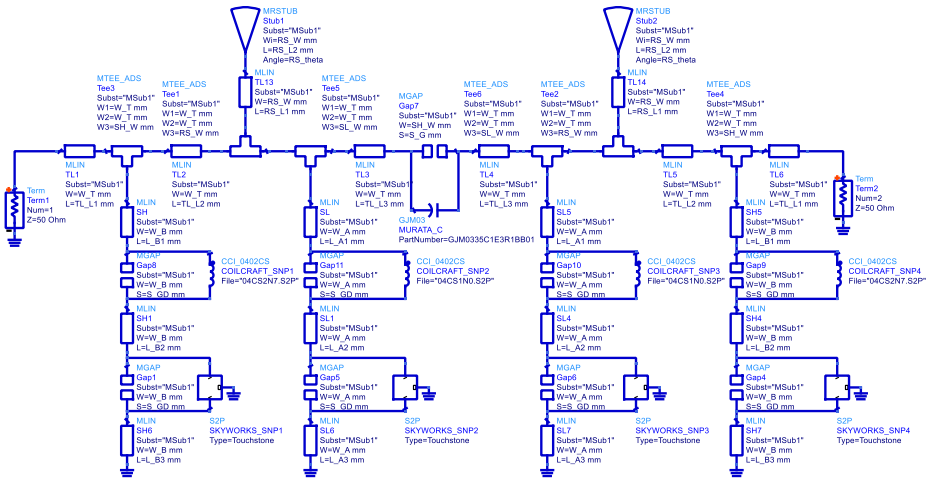

Fig. 5. Schematic of the reconfigurable NRI-TL phase shifter in Keysight – Advanced Design System (ADS). Realistic S-parameter models of the lumped LC components from Murata and Coilcraft were used, together with S-parameter models from Skyworks for the OFF and ON states of the PIN diodes.

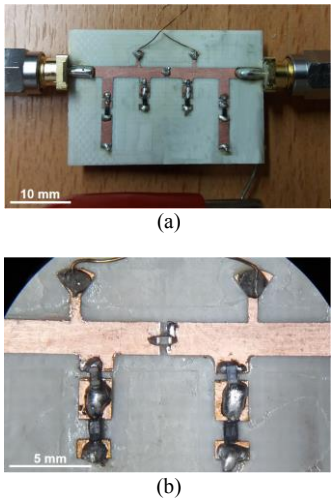

(a)

(b)

Fig. 6. (a) Fabricated prototype of the proposed reconfigurable NRI-TL phase shifter, (b) zoomed-in view of the central unit cell.

the microstrip lines and gaps on a Rogers RO4003C substrate (ε_r = 3.38, tanδ = 0.0027, h = 0.813 mm), as can be seen in the full simulation models of Figs 4 and 5. For a two-state insertion phase of $\phi_{MTM\_A} = -15°$ in *State A* and of $\phi_{MTM\_B} = +60°$ in *State B*, the final optimized set of loading values was determined to be C_0 = 3.1 pF, $2L_{0A}$ = 1.1 nH, and $2L_{0B}$ = 2.8 nH, corresponding to available discrete values in the Murata GJM03 and the Coilcraft 0402CS component series. It is worth mentioning here that the total shunt inductance for a particular state is a combination of the loading inductance (L_{0A} or L_{0B}), the internal inductance of the Skyworks diodes (L_{PIN} = 0.7 nH) and the physical dimensions of the corresponding stub (*Stub A* or *Stub B*). The final layout dimensions of the phase shifter are also listed in Table I.

The fabricated prototype of the proposed reconfigurable NRI-TL phase shifter is presented in Fig 6(a). First, the microstrip conductor and gap patterns shown of Fig. 4 were realized on the Rogers RO4003C substrate using a LPKF ProtoMat H100 milling machine. Holes of 0.4 mm diameter were drilled at the end of all four stubs for the placement of shorting vias. Then, the lumped components (C_0, $2L_{0A}$ and $2L_{0B}$) and diodes (D^+ and D^-) were soldered onto the microstrip transmission lines, as shown in the zoomed-in view of the central metamaterial unit cell in Fig. 6 (b). Finally, SMA connectors were attached for the S-parameter measurements.

To achieve reconfigurability, a Skyworks SMP1345 PIN diode was used, which achieves ON and OFF states based on the biasing polarity. It is important to note that the polarity of the diode on *Stub A* (D^-) is opposite to the polarity of the diode on *Stub B* (D^+). Negative biasing through the radial stubs (l_{rs}, w_{rs}, r_{rs}, and θ_{rs}) along the top of the microstrip line in Fig. 4 turns on the two diodes D^-, and turns off the two diodes D^+, thus defining *State A*. Similarly, positive biasing through the radial stubs reverses this operation, consequently defining *State B*. The DC ground for the differential diode biasing voltage is applied on the microstrip ground and is applied to the diodes through the grounding vias at the end of the stubs.

Surface-mount Murata chip capacitors (GJM03 series) and Coilcraft chip inductors (0402CS series), both with high self-resonant frequencies well above the operating frequency, were used in the realization of the phase shifter. It is important to mention that the achievable phase states rely on the available lumped-element component values in the Murata GJM03 series and the Coilcraft 0402CS series component libraries. The gaps g_1 and g_2 wre designed keeping in mind the recommended soldering footprint for each lumped-element component and the diodes.

Finally, Keysight – ADS was used to design and analyze the performance of the proposed reconfigurable NRI-TL phase shifter using realistic S-parameter models for the Murata capacitors, the Coilcraft inductors and the Skyworks diodes, in conjunction with a realistic model of the physical geometry of the microstrip lines and gaps on a Rogers RO4003C substrate (ε_r = 3.38, tanδ = 0.0027, h = 0.813 mm), as can be seen in the full simulation models of Figs 4 and 5. For a two-state insertion phase of $\phi_{MTM\_A} = -15°$ in *State A* and of $\phi_{MTM\_B} = +60°$ in *State B*, the final optimized set of loading values was determined to be C_0 = 3.1 pF, $2L_{0A}$ = 1.1 nH, and $2L_{0B}$ = 2.8 nH, corresponding to available discrete values in the Murata GJM03 and the Coilcraft 0402CS component series. It is worth mentioning here that the total shunt inductance for a particular state is a combination of the loading inductance (L_{0A} or L_{0B}), the internal inductance of the Skyworks diodes (L_{PIN} = 0.7 nH) and the physical dimensions of the corresponding stub (*Stub A* or *Stub B*). The final layout dimensions of the phase shifter are also listed in Table I.

The fabricated prototype of the proposed reconfigurable NRI-TL phase shifter is presented in Fig 6(a). First, the microstrip conductor and gap patterns shown of Fig. 4 were realized on the Rogers RO4003C substrate using a LPKF ProtoMat H100 milling machine. Holes of 0.4 mm diameter were drilled at the end of all four stubs for the placement of shorting vias. Then, the lumped components (C_0, $2L_{0A}$ and $2L_{0B}$) and diodes (D^+ and D^-) were soldered onto the microstrip transmission lines, as shown in the zoomed-in view of the central metamaterial unit cell in Fig. 6 (b). Finally, SMA connectors were attached for the S-parameter measurements.

VI. Results And Discussion

The simulated and measured results of the reconfigurable NRI-TL phase shifter are shown in Fig. 7, where it can be

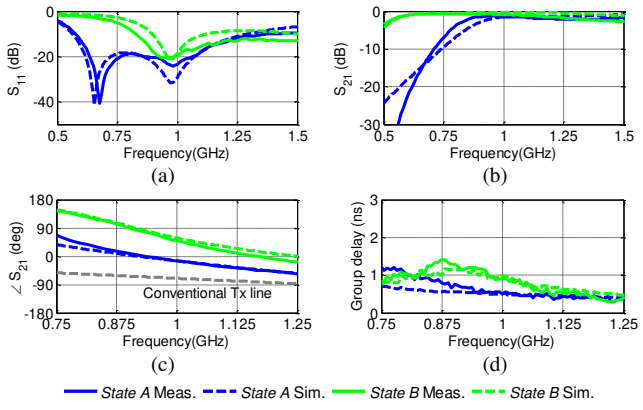

Fig. 7. Simulated and measured responses of the reconfigurable NRI-TL metamaterial phase shifter. (a) $|S_{11}|$, (b) $|S_{21}|$, (c) phase of S_{21}, and (d) group delay.

observed that there is very good correlation between the two. The reflection coefficients for both S*tate A* and *State B* shown in Fig. 7(a) are well below −10 dB at 1 GHz, indicating good impedance matching at the design frequency. At 1 GHz, the simulated and measured $|S_{11}|$ are −18.34 dB and −19.33 dB, respectively for *State A*, while they are −29.05 dB and −23.38 dB, respectively for *State B*. The advantages achieved by excluding the tuning mechanism from the direct signal path can be witnessed in terms of the low insertion losses, seen in Fig. 7(b). The simulated and measured $|S_{21}|$ are −1.53 dB and −1.43 dB, respectively for *State A*, and −0.23 dB and −0.89 dB, respectively for *State B*. In Fig. 7(c), the phase response of an unloaded microstrip line is compared with the simulated and measured phase responses for both *State A* and *State B*. From Fig. 7(a), (b) and (c), it can be observed that the reconfigurable NRI-TL metamaterial phase shifter retains its good impedance matching and transmission characteristics even though the insertion phase is significantly changed from *State A* to *State B*. At 1 GHz, the transmission line phase shift of $\phi_{H\text{-}TL} = -70^\circ$ is compensated by $\phi_{BW} = 55.5^\circ$ and 128.5° for *State A* and *State B*, respectively (as discussed in Section III), resulting in $\phi_{MTM\_A} = -14.5^\circ$ and $\phi_{MTM\_B} = +58.5^\circ$ at 1 GHz. The measured phase shift deviates by 2.4% and 0.03% from the predicted simulated value for *State A* and *State B,* respectively, which is well within the fabrication tolerances. Although the difference between the simulated and measured phase responses is relatively small, cascaded phase shifters and phase sensitive systems like Directional Modulation (DM) antenna arrays demand more accuracy. This error can be associated with the observable fabrication anomalies especially at the transition between the transmission line and the stubs, caused due to the limitations of the in-house fabrication facilities, as highlighted in Fig. 6(b). The measured phase error can be further decreased by a more careful and controlled fabrication of the microstrip traces, for example using wet etching and photolithography. The group delay of the reconfigurable NRI-TL phase shifter is shown in Fig. 7(d), depicting good simulation and measurement agreement for both states. At 1 GHz, the measured group delay is 0.5 ns for *State A*, and 0.9 ns for *State B*, and these remain relatively flat in the range of 0.4 ns to 1.3 ns across the operating band shown.

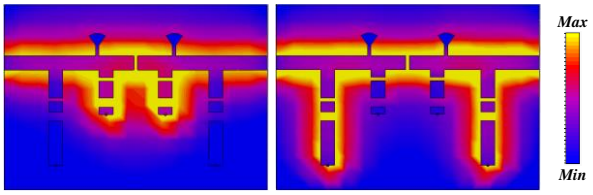

Fig. 8. Normalized surface current distribution at 1 GHz on the conductors of the NRI-TL metamaterial phase shifter in (a) *State A*, and (b) *State B*.

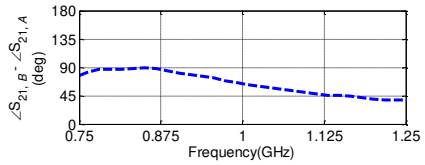

Fig. 9. Measured phase difference between the two states.

TABLE II
RANGE ANALYSIS OF THE RECONFIGURABLE NRI-TL METAMATERIAL PHASE SHIFTERS

ϕ_{BW_A}	ϕ_{BW_B}	Desired ΔΦ	ϕ_{MTM_A}	ϕ_{MTM_B}	Realized ΔΦ	Phase deviation
20°	40°	20°	-50.69°	-30.08°	20.61	0.19 %
40°	80°	40°	-29.69°	+10.06°	39.75	0.09 %
60°	120°	60°	-10.01°	+52.97°	62.98	0.83 %
80°	160°	80°	+10.97°	+89.40°	78.43	0.27 %

Fig. 8 shows the surface current distribution on the conductors of the reconfigurable NRI-TL phase shifter for *State A* and *State B*. It can be observed that the maximum surface current resides within the defined NRI-TL metamaterial unit cell for a particular state, while the un-used stubs carry an insignificant amount of surface current, resulting in very good isolation in both states. The measured phase difference between the two states, $\Delta\Phi = \angle S_{21,B} - \angle S_{21,A}$, is shown in Fig. 9, where it can be observed that it is relatively flat with a value of 73° at 1 GHz that varies between 38.4° to 89.1° in the range shown. Although the operational range of the proposed algorithm in Section IV depends upon the acceptable tolerance factor for any given application, an overview has been presented in Table II where the proposed algorithm was tested for a range of ϕ_{BW}(s) for both states while Z_0, d and f_0 were kept the same as they were in the solution presented in Fig. 4 and Table I. The resulting set of ϕ_{MTM}(s) for both states are shown in Table II, where it is evident that the phase deviation from the intended ϕ_{MTM} remains below 1% for ϕ_{BW_A} as low as 20° and ϕ_{BW_B} as high as 160°. On the other hand, the algorithm still converged when ϕ_{BW_A} and ϕ_{BW_B} were 100° and 200° respectively, while the phase deviation was 10.25% from the intended phase difference. Despite the different phase differences the overall size of the phase-shifter's transmission line does not change. Finally, Table III summarizes the performance of the proposed reconfigurable NRI-TL metamaterial phase shifter and other phase shifters found in the literature, which compares quite favorably. It has the most compact size (0.07 λ × 0.06 λ) when normalized with respect to the central frequency wavelength, the widest bandwidth (18.7%) within which the phase of S_{21} varies less than ± 20°, and has the lowest insertion loss amongst the phase shifters implemented with lumped surface-mount components. Albeit its compact and simple structure, one of the major disadvantages of the proposed architecture is the discrete phase shift that it can achieve.

TABLE III
PERFORMANCE COMPARISON OF RECONFIGURABLE NRI-TL METAMATERIAL BASED PHASE SHIFTERS

Ref	[7]	[8]	[9-10]	[14]	This work
Size (mm×mm)	30.0×68.0	85.5×30.0	10.8×9.4	30.0×40.0	17.8×21.6
Size (λ × λ)	0.19×0.09	0.57×0.20	0.09×0.08	0.26×0.20	0.07×0.06
Freq (GHz)	0.9	2.0	2.5	2.0	1.0
IL (dB) min-max	4.0-5.6	0.56-0.69	0.55-1.1	2-10	0.89-1.43
Phase range min-max	-22° to 30°	313° to 355°	-40° to 34°	51° to 184°	-14° to 59°
Bandwidth $\angle S_{21} \pm 20°$	0.83-0.95* 13.5%	2.00-2.08* 3.9%	2.40-2.70* 11.8%	2.40-2.75* 13.6%	0.92-1.11 18.7%
Technology	Micro-fluids	metallic perturber	MMIC inductor & varactor diode	varactor diode	PIN diode

* estimated from graphs

Other topologies that have achieved continuous phase tuning capabilities can be found in [8-10]. An extension of this work would be to apply existing continuous phase tuning methods to the architecture proposed herein.

VII. CONCLUSION

A novel architecture of a reconfigurable phase-shifter based on NRI-TL metamaterial unit cells has been presented that is compact in size and exhibits low insertion loss characteristics. By modeling and optimizing two collocated NRI-TL metamaterial Π unit cells loaded with the same series capacitance but different shunt inductances, two distinct phase states have been achieved. It has been shown that by decreasing the shunt inductance in an NRI-TL unit cell to achieve a higher phase shift while using the same series capacitance, disturbs the matching of the unit cell severely. Good matching has been achieved in both phase states by adjusting the length and positions of the inductively-loaded shorted stubs. The reconfigurable mechanism has been achieved by placing PIN diodes on four shorted stubs, enabling the device to operate in two phase states based on the biasing polarity. This also avoids the presence of lossy components in the direct signal path. The proposed device was fabricated on a 17.8 × 21.6 mm^2 Rogers RO4003C substrate and the measured results show good agreement with the simulations. The useable bandwidth of the proposed device for which the $|S_{11}|$ of both states simultaneously remains below −10 dB is 0.46 GHz (46%), from 0.83 GHz to 1.29 GHz. In *State A*, the phase shifter achieves a phase shift of −14.5°, while in *State B* +58.5°, resulting in a measured differential phase shift of 73° at 1 GHz. The measured $|S_{21}|$ for *State A* is −1.43 dB, and for *State B* −0.89 dB. The realized phase difference is representative, and the same metamaterial phase-shifting architecture can also be used to achieve any arbitrary phase shifting value till $\Delta\Phi = 90°$. Thus, the proposed reconfigurable NRI-TL metamaterial phase-shifter is ideal for use in feeding networks of next-generation antenna array systems for pattern and polarization diversity applications. Also, the capability to achieve high phase differences makes it well suited for use in massive MIMO systems since the compact foot print of the proposed phase shifter is easy to be accommodated within the limited space left in a massive MIMO system, which includes a large number of radiating elements. In addition, despite the different phase differences the overall physical dimensions of the phase-shifter's transmission line remain unchanged and thus rather compact. Most importantly, the phase shifter, because of its small size compared to the wavelength at f_0 does not radiate itself, and therefore it does not perturb the radiation pattern of the array, even when it is implemented on the same layer as the radiating elements.

REFERENCES

[1] G. Oliveri, D. H. Werner and A. Massa, "Reconfigurable electromagnetics through metamaterials—A review," *Proc. IEEE*, vol. 103, no. 7, pp. 1034-1056, Jul. 2015.
[2] G.V. Eleftheriades, A.K. Iyer, and P.C. Kremer, "Planar negative refractive index media using periodically L-C loaded transmission lines," *IEEE Trans. Microw. Theory Tech.*, vol. 50, no. 12, pp. 2702–2712, Dec. 2002.
[3] M. A. Antoniades and G. V. Eleftheriades, "Compact linear lead/lag metamaterial phase shifters for broadband applications," *IEEE Antennas Wireless Propag. Lett.*, vol. 2, no. 1, pp. 103-106, May. 2003.
[4] S. I. M. Sheikh *et al*., "Analog/digital ferrite phase shifter for phased array antennas," *IEEE Antennas and Wireless Propag. Lett.*, vol. 9, no. 1, pp. 319-321, Apr. 2010.
[5] W. W. G. Hui, J. M. Bell, M. F. Iskander and J. J. Lee, "Low-cost microstrip-line-based ferrite phase shifter design for phased array antenna applications," *IEEE Antennas and Wireless Propag. Lett.*, vol. 6, no. 1, pp. 86-89, Mar. 2007.
[6] P. Y. Chen, C. Argyropoulos and A. Alù, "Terahertz antenna phase shifters using integrally-gated graphene transmission-lines," *IEEE Trans. Antennas Propag.*, vol. 61, no. 4, pp. 1528-1537, Apr. 2013.
[7] S. Choi, W. Su, M. M. Tentzeris and S. Lim, "A novel fluid-reconfigurable advanced and delayed phase line using inkjet-printed microfluidic composite right/left-handed transmission line," *IEEE Microw. Wireless Compon. Lett.*, vol. 25, no. 2, pp. 142-144, Feb. 2015.
[8] N. Michishita, H. Kitahara, Y. Yamada and K. Cho, "Tunable phase shifter using composite right/left-handed transmission line with mechanically variable MIM capacitors," *IEEE Antennas Wireless Propag. Lett.*, vol. 10, pp. 1579-1581, Dec. 2011.
[9] M. A. Y. Abdalla, K. Phang and G. V. Eleftheriades, "A 0.13-um CMOS phase shifter using tunable positive/negative refractive index transmission lines," *IEEE Microw. Wireless Compon. Lett.*, vol. 16, no. 12, pp. 705-707, Dec. 2006.
[10] M. A. Y. Abdalla, K. Phang and G. V. Eleftheriades, "Printed and integrated CMOS positive/negative refractive-index phase shifters using tunable active inductors," *IEEE Trans. Microw. Theory Tech.*, vol. 55, no. 8, pp. 1611-1623, Aug. 2007.
[11] M. Durán-Sindreu *et al*., "Electrically tunable composite right/left handed transmission-line based on open resonators and Barium-Stronium-Titanate thick films," in *Proc. IEEE MTT-S Int. Microw. Symp.*, Jun. 2011, pp. 1-4.
[12] H. Kim, A. B. Kozyrev, A. Karbassi and D. W. van der Weide, "Linear tunable phase shifter using a left-handed transmission line," *IEEE Microw. Wireless Compon. Lett.*, vol. 15, no. 5, pp. 366-368, May 2005.
[13] H. Kim, A. B. Kozyrev, A. Karbassi and D. W. van der Weide, "Compact left-handed transmission line as a linear phase–voltage modulator and efficient harmonic generator," *IEEE Trans. Microw. Theory Tech.*, vol. 55, no. 3, pp. 571-578, Mar. 2007.
[14] C. Damm, M. Schussler, M. Oertel and R. Jakoby, "Compact tunable periodically LC loaded microstrip line for phase shifting applications," in *Proc. IEEE MTT-S Int. Microw. Symp.*, Jun. 2005, pp. 2003 – 2006.
[15] D. Kuylenstierna, A. Vorobiev, P. Linner and S. Gevorgian, "Composite right/left handed transmission line phase shifter using ferroelectric varactors," *IEEE Microw. Wireless Compon. Lett.*, vol. 16, no. 4, pp. 167-169, Apr. 2006.
[16] J. Perruisseau-Carrier, K. Topalli and T. Akin, "Low-loss Ku-band artificial transmission line with MEMS tuning capability," *IEEE Microw. Wireless Compon. Lett.*, vol. 19, no. 6, pp. 377-379, Jun. 2009.
[17] M. A. Antoniades, H. Mirzaei, and G. V. Eleftheriades, "Transmission-line based metamaterials in antenna engineering," in *Handbook of Antenna Technologies*, Z. N. Chen, Ed. Singapore: Springer Science, Jul. 2015.